Exciton Structure and Zeeman Effects in Cadmium Selenide*†

R. G. WHEELER AND J. O. DIMMOCK‡

Sloane Physics Laboratory, Yale University, New Haven, Connecticut

(Received August 10, 1961)

The exciton spectra of CdSe has been observed and identified by optical reflection, absorption and Zeeman structure at 1.8°K. The reflection and absorption spectra indicate the presence of two nonoverlapping exciton series. From observed optical selection rules, the conduction band is identified as having Γ_7 symmetry. The two series correspond to the Γ_9 and Γ_7 valence bands split by the crystal field by approximately 200 cm^{-1}. A third series, at higher energies, has been observed in absorption corresponding to a Γ_7 valence band state split by spin-orbit effects from the other two states by approximately 3490 cm^{-1}. The $n_1 = 1$, 2, 3, and 4 states of the first (Γ_9) series, the $n_2 = 1$ and 2 states of the second (first Γ_7) series, and the $n_3 = 1$ state of the third (second Γ_7) series have been observed and identified in absorption. The series limit of the first series, corresponding to the band gap, has been measured to be 14 850 cm^{-1}. A semi-empirical theory of exciton structure in the presence of an external magnetic field developed in the effective mass approximation has been used to obtain the band parameters at $K = 0$ of CdSe from observed exciton spectra. The effect of the finite photon momentum has been observed through changes in the Zeeman structure of the $n_1 = 2$, P states upon 180° rotation of the magnetic field in the plane perpendicular to the crystal C axis. Some deviations between experiment and the theoretical predictions of the ellipsoidal effective mass theory have been observed. The relation between these deviations and the possibility of toroidal energy surfaces in CdSe is discussed briefly.

INTRODUCTION

THE observation and interpretation of the exciton spectra in semiconductors gives detailed information concerning the electronic band structure of the material in question. This is to report on such observations in wurtzite cadmium selenide.[1] The identification and subsequent interpretation was facilitated by measurements of the magneto-optical effects of the spectra. A qualitative understanding of the spectra is obtained from a review of the allowed band symmetries at $K = 0$ in crystals of C_{6v}^4 symmetry. The exciton symmetries and selection rules are obtained group theoretically. A quantitative comparison with an anisotropic exciton mass theory, which will be outlined, permits evaluation of the electron and hole mass and g-value parameters.

As pointed out by Birman,[2] Glasser,[3] and others, if one considers the valence band as P-like and the conduction band as S-like in the II-VI wurtzite class of semiconductors, at $K = 0$ the conduction band including spin will have a Γ_7 symmetry, and the valence band will be split into three doubly degenerate states with the symmetries Γ_9, Γ_7, and Γ_7. The valence band splitting is due to the spin-orbit and crystal field effects. The exciton states then will reflect these symmetries, as well as the symmetries of the hydrogenic state of the exciton in the center of mass.[4,5] The states observable by dipole radiation will be those whose representation[6] is either Γ_1 or Γ_5 corresponding to polarizations $\mathbf{E} \| \mathbf{C}$ and $\mathbf{E} \perp \mathbf{C}$, respectively. These remarks are summarized in Fig. 1 for S-, P-, and D-hydrogenic states.

Using the $\mathbf{K} \cdot \mathbf{p}$ method to second order, Casella[7] and Rashba and Sheka[8] have shown that the secular determinant specifying the energy surface for bands of Γ_7 symmetry may contain linear off-diagonal terms. These terms give rise to a linear K dependence of the band energy resulting in a toroidal energy surface which has its minima away from $K = 0$. The determinant applicable for bands of Γ_9 symmetry contains only diagonal quadratic terms. Thus in the effective-mass approximation for exciton states, the defining equation may be written as a Hamiltonian matrix deduced from the secular determinants defining the relevant band edges.[4,9] The ellipsoidal approximation is defined as the case which neglects all off-diagonal terms in the Hamiltonian matrix, and considers the diagonal ones

Bands	Exciton Symmetry	
	Γ_7 Conduction Band	Γ_7 Conduction Band
Γ_7	Γ_9 Valence Band	Γ_7 Valence Band
GAP	$S \quad \Gamma_5 + \Gamma_6$	$S \quad \Gamma_1 + \Gamma_2 + \Gamma_5$
	$P_0 \quad \Gamma_5 + \Gamma_6$	$P_0 \quad \Gamma_1 + \Gamma_2 + \Gamma_5$
Γ_9	$P_{\pm 1} \quad \Gamma_1 + \Gamma_2 + \Gamma_3 + \Gamma_4 + \Gamma_5 + \Gamma_6$	$P_{\pm 1} \quad \Gamma_1 + \Gamma_2 + 2\Gamma_5 + \Gamma_6$
Γ_7	$D_0 \quad \Gamma_5 + \Gamma_6$	$D_0 \quad \Gamma_1 + \Gamma_2 + \Gamma_5$
	$D_{\pm 1} \quad \Gamma_1 + \Gamma_2 + \Gamma_3 + \Gamma_4 + \Gamma_5 + \Gamma_6$	$D_{\pm 1} \quad \Gamma_1 + \Gamma_2 + 2\Gamma_5 + \Gamma_6$
Γ_7	$D_{\pm 2} \quad \Gamma_1 + \Gamma_2 + \Gamma_3 + \Gamma_4 + \Gamma_5 + \Gamma_6$	$D_{\pm 2} \quad \Gamma_3 + \Gamma_4 + \Gamma_5 + 2\Gamma_6$
$K = 0,0,0$		

FIG. 1. The band symmetries and their relative energies are indicated as is compatible with the observed optical selection rules for three exciton series in cadmium selenide. With the light polarization parallel and perpendicular to the C axis, dipole transitions to the Γ_1 and Γ_5 states, respectively, are allowed.

[1] Gross, *et al.*, have also reported on the observation of lines in the absorption edge of CdSe, however without identification. E. F. Gross and V. V. Sobolev, Zhur. tech. Fiz. **26**, 1622 (1956).

[2] J. L. Birman, Phys. Rev. Letters **2**, 157 (1959); Phys. Rev. **114**, 1490 (1959).

[3] M. L. Glasser, J. Phys. Chem. Solids **10**, 229 (1959).

[4] G. Dresselhaus, J. Phys. Chem. Solids **1**, 14 (1956).

[5] H. Haken, J. Phys. Chem. Solids **8**, 166 (1959).

[6] V. Heine, *Group Theory in Quantum Mechanics* (Pergamon Press, New York, 1960).

[7] R. C. Casella, Phys. Rev. Letters **5**, 371 (1960).

[8] E. I. Rashba and B. I. Sheka, Fiz. Iverd. Tela, Collected Articles **2**, 162 (1959).

[9] J. M. Luttinger and W. Kohn, Phys. Rev. **97**, 869 (1955).

to be equal. This model will describe the experimental results if the following assumptions characterize the properties of cadmium selenide.

1. The band extrema are at or very near $\mathbf{K}=0$. Their shape is parabolic with the double degeneracy carried at least to second order in $\mathbf{K}$. With this assumption one may write the exciton equation as a simple hydrogenic Schrödinger equation including mass and dielectric anisotropy. These anisotropies are cylindrical with the crystal C axis, the axis of rotation.

2. The resultant exciton mass anisotropy is small, allowing first-order perturbation calculations to be made for the energy states as well as for the magnetic field effects.

3. The valence band splittings are larger than the exciton binding energies allowing one to neglect mixing between valence bands.

4. The energy of the longitudinal optical phonon is much greater than the exciton binding energy, allowing low-frequency dielectric constants to be used in the calculations with no corrections for polaron effects.[5,10]

The ellipsoidal model is still useful even when one or more of the above assumptions is invalid. If the deviations are small one can include their effect as a perturbation.

The observed spectra has been interpreted on the basis of this model. Deviations are observed which are discussed in terms of the possibility of toroidal energy surfaces of the Γ_7 bands. Finally, electron g values obtained are compared with the theory of Roth et al.[11,12]

THEORY

In the ellipsoidal model the effective-mass Hamiltonian for an exciton in the presence of an external magnetic field can conveniently be considered as a sum of terms.[4,13]

$$\mathcal{3C}=\mathcal{3C}_1+\mathcal{3C}_2+\mathcal{3C}_3+\mathcal{3C}_4+\mathcal{3C}_{K1}+\mathcal{3C}_{K2}+\mathcal{3C}_{K3}, \quad (1)$$

where

$$\mathcal{3C}_1=-\frac{\hbar^2}{2m}\left\{\frac{1}{\mu_x}\frac{\partial^2}{\partial x^2}+\frac{1}{\mu_x}\frac{\partial^2}{\partial y^2}+\frac{1}{\mu_z}\frac{\partial^2}{\partial z^2}\right\}$$
$$-\frac{e^2}{\epsilon\eta^{\frac{1}{2}}}(x^2+y^2+\eta^{-1}z^2)^{-\frac{1}{2}}, \quad (2)$$

$$\mathcal{3C}_2=-2i\beta_0\left\{\frac{A_x}{\Delta_x}\frac{\partial}{\partial x}+\frac{A_y}{\Delta_x}\frac{\partial}{\partial y}+\frac{A_z}{\Delta_z}\frac{\partial}{\partial z}\right\}, \quad (3)$$

[10] T. Muto, Suppl. Progr. Theoret. Phys. (Japan) 12, 3 (1959).
[11] L. M. Roth, B. Lax, and S. Zwerdling, Phys. Rev. 114, 90 (1959).
[12] L. M. Roth, Phys. Rev. 118, 1534 (1960).
[13] The Hamiltonian is written in the following coordinate system

$$\mathbf{R}=\tfrac{1}{2}(\mathbf{r}_e+\mathbf{r}_h),$$
$$\mathbf{r}=\mathbf{r}_e-\mathbf{r}_h,$$

which is the coordinate system used by Dresselhaus. This system was chosen because one cannot define a center of mass transformation for excitons formed from degenerate bands in the general case. The relative coordinate, $\mathbf{r}$, is the one which appears in the formalism.

$$\mathcal{3C}_3=\frac{e^2}{2mc^2}\left\{\frac{1}{\mu_x}A_x^2+\frac{1}{\mu_x}A_y^2+\frac{1}{\mu_z}A_z^2\right\}, \quad (4)$$

$$\mathcal{3C}_4=\tfrac{1}{2}\beta_0\sum_{\gamma=x,y,z}(g_{e\gamma}s_{e\gamma}+g_{h\gamma}s_{h\gamma})H_\gamma, \quad (5)$$

$$\mathcal{3C}_{K1}=-\frac{i\hbar^2}{2m}\left\{\frac{K_x}{\Delta_x}\frac{\partial}{\partial x}+\frac{K_y}{\Delta_x}\frac{\partial}{\partial y}+\frac{K_z}{\Delta_z}\frac{\partial}{\partial z}\right\}, \quad (6)$$

$$\mathcal{3C}_{K2}=\beta_0\left\{\frac{K_x}{\mu_x}A_x+\frac{K_y}{\mu_x}A_y+\frac{K_z}{\mu_z}A_z\right\}, \quad (7)$$

$$\mathcal{3C}_{K3}=\frac{\hbar^2}{8m}\left\{\frac{1}{\mu_x}K_x^2+\frac{1}{\mu_x}K_y^2+\frac{1}{\mu_z}K_z^2\right\}, \quad (8)$$

in which m is the free-electron mass, μ_γ is the reduced effective mass of the exciton in the direction γ,

$$\frac{1}{\mu_\gamma}=\left(\frac{m}{m_{e\gamma}^*}+\frac{m}{m_{h\gamma}^*}\right),$$

with $m_{e\gamma}^*$ and $m_{h\gamma}^*$ respectively the electron and hole effective masses in the direction γ. Also

$$\beta_0=e\hbar/2mc,$$
$$\mathbf{A}=\tfrac{1}{2}(\mathbf{H}\times\mathbf{r}),$$

and

$$\frac{1}{\Delta_\gamma}=\left(\frac{m}{m_{e\gamma}^*}-\frac{m}{m_{h\gamma}^*}\right).$$

Since we assume that the valence and conduction band extrema are at $\mathbf{K}=0$, the wave vector of the light which creates the exciton is $\mathbf{K}$ which represents the position of the exciton in K space. One recognizes the origin of the terms to be as follows. $\mathcal{3C}_1$ is the Hamiltonian for a hydrogenic system in the absence of external fields with the possibility of mass and dielectric anisotropies included. The dielectric constant transverse to the crystal c axis (taken as the z direction) is ϵ, and $\epsilon\eta$ is the dielectric constant in the z direction. $\mathcal{3C}_2$ is the linear (Zeeman) magnetic field term. $\mathcal{3C}_3$ is the quadratic (diamagnetic) magnetic field term. $\mathcal{3C}_4$ is a convenient representation of the spin energy in the presence of an external magnetic field. We note that due to the small effective reduced mass of the exciton and the large dielectric constant of CdSe, the radii of the exciton states will be much larger than the corresponding hydrogen state radii. Hence since spin-orbit and spin-spin coupling is proportional to r^{-3} and is thus quite small, it is legitimate to write the magnetic field perturbations in the above Paschen-Bach limit. The last three terms are the familiar $\mathbf{K}\cdot\mathbf{p}$ term, the $\mathbf{K}\cdot\mathbf{A}$ term due to the magnetic field, and the familiar K^2 term, respectively. If the exciton Hamiltonian is written in the center-of-effective-mass system, the $\mathbf{K}\cdot\mathbf{p}$ term may be eliminated and the K^2 term cast in

the form,

$$E_K = \frac{\hbar^2}{2}\left\{\frac{1}{M_x}K_x{}^2 + \frac{1}{M_x}K_y{}^2 + \frac{1}{M_z}K_z{}^2\right\}, \qquad (9)$$

where

$$M_\gamma = (m_{e\gamma}{}^* + m_{h\gamma}{}^*).$$

We, however, retain the present form and will choose as zero-order basis functions those which permit this simplification.

It will be convenient to consider the total Hamiltonian, $\mathcal{3C}$, as a zero-order Hamiltonian, $\mathcal{3C}_0$, plus perturbation terms. $\mathcal{3C}_1$ is written in the following form:

$$\mathcal{3C}_1 = \mathcal{3C}_0 + \mathcal{3C}_\alpha,$$

where

$$\mathcal{3C}_0 = -\frac{\hbar^2}{2m}\left\{\frac{1}{\mu_x}\left(\frac{\partial^2}{\partial x^2} + \frac{\partial^2}{\partial y^2}\right) + \frac{1}{\mu_z}\frac{\partial^2}{\partial z^2}\right\}$$
$$-\frac{e^2}{\epsilon\eta^{\frac{1}{2}}}\left(x^2 + y^2 + \frac{\mu_z}{\mu_x}z^2\right)^{-\frac{1}{2}}, \quad (10)$$

$$\mathcal{3C}_\alpha = -\frac{e^2}{\epsilon\eta^{\frac{1}{2}}}\left\{(x^2 + y^2 + \eta^{-1}z^2)^{-\frac{1}{2}} - \left(x^2 + y^2 + \frac{\mu_z}{\mu_x}z^2\right)^{-\frac{1}{2}}\right\}. \quad (11)$$

The zero-order state functions which satisfy the equation

$$\mathcal{3C}_0\Phi_j = E_j{}^0\Phi_j \qquad (12)$$

are related to the hydrogenic state functions, Ψ_j, by

$$\Phi_j(x,y,z) = (\mu_z/\mu_x)^{\frac{1}{2}}\Psi_j(x,y,(\mu_z/\mu_x)^{\frac{1}{2}}z), \qquad (13)$$

on a scale where the first Bohr orbit is

$$a_0' = (\hbar^2/me^2)(\epsilon/\mu_x)\eta^{\frac{1}{2}} = a_0(\epsilon/\mu_x)\eta^{\frac{1}{2}}. \qquad (14)$$

The energy $E_j{}^0$ is related to the energy of the corresponding state in the hydrogen atom by[14]

$$E_j{}^0 = (\mu_x/\epsilon^2\eta)E_j{}^{\mathrm{H}}. \qquad (15)$$

It will be convenient in calculating matrix elements to use the hydrogenic functions $\Psi_j(x,y,z)$ instead of $\Phi_j(x,y,z)$. The matrix elements of the operator $\mathbf{Q}(x,y,z)$ can be written as

$$\langle\Phi_i(x,y,z)|\mathbf{Q}(x,y,z)|\Phi_j(x,y,z)\rangle$$
$$= \langle\Psi_i(x,y,z)|\mathbf{Q}(x,y,(\mu_x/\mu_z)^{\frac{1}{2}}z)|\Psi_j(x,y,z)\rangle$$
$$= \langle i|\mathbf{Q}(x,y,(\mu_x/\mu_z)^{\frac{1}{2}}z)|j\rangle$$
$$= \langle i|\mathbf{Q}'|j\rangle, \qquad (16)$$

and are most easily computed when written in this

form. The prime indicates that the operator has been transformed.

The anisotropy perturbation is obtained from the matrix elements

$$\langle i|\mathcal{3C}_\alpha'|j\rangle.$$

The calculation is facilitated by writing

$$\mathcal{3C}_\alpha' = (e^2/\epsilon\eta^{\frac{1}{2}}r)[1 - (1 - \alpha\cos^2\theta)^{-\frac{1}{2}}], \qquad (17)$$

where

$$\alpha = 1 - \mu_x\epsilon_x/\mu_z\epsilon_z = 1 - \mu_x/\mu_z\eta.$$

Since we expect the perturbation approach to be accurate only to first order and then only if α is small, the actual calculations may be made from the expansion

$$\mathcal{3C}_\alpha' = -(e^2/\epsilon\eta^{\frac{1}{2}}r)(\tfrac{1}{2}\alpha\cos^2\theta + \tfrac{3}{8}\alpha^2\cos^4\theta + \cdots). \quad (18)$$

The selection rules for this operator are

$$l_i - l_j = \text{even}, \quad m_i - m_j = 0.$$

These matrix elements, as well as those for the magnetic field perturbations, can be obtained by standard means and hence will not be presented here. Instead only the transformed operators and selection rules will be given.[15]

In the case where $\mathbf{H}\|\mathbf{C}$, the linear magnetic field perturbation is obtained from

$$\mathcal{3C}_2' = \beta_0\frac{1}{\Delta_x}H_zL_z, \qquad (19)$$

where

$$L_z = -i\left(x\frac{\partial}{\partial y} - y\frac{\partial}{\partial x}\right),$$

which has the selection rules

$$n_i - n_j = l_i - l_j = m_i - m_j = 0.$$

The quadratic terms for $\mathbf{H}\|\mathbf{C}$ are obtained from the operator

$$\mathcal{3C}_3' = \frac{1}{8}\frac{e^2}{mc^2}\frac{1}{\mu_x}H_z{}^2(x^2 + y^2), \qquad (20)$$

which has the selection rules

$$l_i - l_j = 0, \pm 2; \quad m_i - m_j = 0.$$

In the case where $\mathbf{H}\perp\mathbf{C}$ ($\mathbf{H}$ along x) the linear magnetic field perturbation takes the form

$$\mathcal{3C}_2' = -i\beta_0\frac{1}{\Delta_x}H_x\left(\frac{\mu_z}{\mu_x}\right)^{\frac{1}{2}}\left(\frac{\Delta_x}{\Delta_z}y\frac{\partial}{\partial z} - \frac{\mu_x}{\mu_z}z\frac{\partial}{\partial y}\right). \qquad (21)$$

---

[14] Different states of the same exciton series are indicated by the letters i, j, etc., such that, for instance, n_i is the principal quantum number of the state i. Since the mixing between different exciton series is not included, being very small, there should be no confusion between this notation and that used to indicate the respective series (n_1, n_2, n_3). The energies E_j of a given series are taken with respect to the appropriate band edge.

[15] There are a number of references for the calculation of matrix elements involving hydrogenic state function. We list here a few of the more general references. H. A. Bethe and E. E. Salpeter, *Quantum Mechanics of One- and Two-Electron Atoms* (Academic Press, Inc., New York, 1957); P. M. Morse and H. Feshbach, *Methods of Theoretical Physics* (McGraw-Hill Book Company, New York, 1953), Vol. I and Vol. II; E. T. Whittaker and G. N. Watson, *Modern Analysis* (Cambridge University Press, New York, 1927), 4th ed.

It is convenient to write this term as follows:

$$\mathcal{K}_2' = \beta_0 \frac{1}{\Delta_x} H_x a L_x - i\beta_0 \frac{1}{\Delta_x} H_x b\left(y\frac{\partial}{\partial z} + z\frac{\partial}{\partial y}\right), \quad (22)$$

where

$$L_x = -i\left(y\frac{\partial}{\partial z} - z\frac{\partial}{\partial y}\right),$$

$$a = \frac{1}{2}\left(\frac{\mu_z}{\mu_x}\right)^{\frac{1}{2}}\left(\frac{\Delta_x}{\Delta_z} + \frac{\mu_x}{\mu_z}\right),$$

$$b = \frac{1}{2}\left(\frac{\mu_z}{\mu_x}\right)^{\frac{1}{2}}\left(\frac{\Delta_x}{\Delta_z} - \frac{\mu_x}{\mu_z}\right).$$

It can be shown that the matrix elements

$$\left\langle i \left| -i\left(y\frac{\partial}{\partial z} + z\frac{\partial}{\partial y}\right) \right| j \right\rangle$$

vanish if $n_i = n_j$. For $n_j \neq n_j$ the contribution due to this term is small enough to be neglected such that the linear magnetic field perturbation for $\mathbf{H} \perp \mathbf{C}$ is obtained from the standard L_x operator. This operator has the selection rules

$$n_i - n_j = l_i - l_j = 0, \quad m_i - m_j = \pm 1.$$

For $\mathbf{H} \perp \mathbf{C}$ the quadratic perturbation takes the form

$$\mathcal{K}_3' = \frac{1}{8}\frac{e^2}{mc^2}\frac{1}{\mu_z} H_x^2(y^2 + z^2), \quad (23)$$

which has the selection rules

$$l_i - l_j = 0, \pm 2; \quad m_i - m_j = 0, \pm 2.$$

We next consider the perturbation due to the $\mathbf{K} \cdot \mathbf{p}$ term.

$$\mathcal{K}_{K1}' = -\frac{i\hbar^2}{2m}\left\{\frac{K_x}{\Delta_x}\frac{\partial}{\partial x} + \frac{K_y}{\Delta_x}\frac{\partial}{\partial y} + \frac{K_z}{\Delta_z}\left(\frac{\mu_z}{\mu_x}\right)^{\frac{1}{2}}\frac{\partial}{\partial z}\right\}. \quad (24)$$

The matrix elements

$$\langle i | \mathcal{K}_{K1}' | j \rangle$$

vanish if $n_i = n_j$. Taking this perturbation to second order we can make use of the sum rule[4,9]

$$\sum_{k}' (E_i^0 - E_k^0)^{-1}\{\langle i | p_\gamma | k\rangle\langle k | p_\lambda | j\rangle + \langle i | p_\lambda | k\rangle\langle k | p_\gamma | j\rangle\} = -m\mu_x \delta_{\gamma\lambda}\delta_{ij}, \quad (25)$$

where

$$E_i^0 = E_j^0 \quad \text{and} \quad \mathbf{p} = -i\hbar\nabla.$$

The perturbation energy, E_{K1}, due to this term is easily seen to be

$$E_{K1} = -(\hbar^2/8m)\{(\mu_x/\Delta_x^2)(K_x^2 + K_y^2) + (\mu_z/\Delta_z^2)K_z^2\}. \quad (26)$$

The perturbation energy, E_{K3}, due to the last term is

$$E_{K3} = H_{K3}' = (\hbar^2/8m)\{(1/\mu_x)(K_x^2 + K_y^2) + (1/\mu_z)K_z^2\}, \quad (8)$$

combining these two terms we obtain to second order in K

$$E_K = E_{K1} + E_{K3} = (\hbar^2/2)\{(1/M_x)(K_x^2 + K_y^2) + (1/M_z)K_z^2\}. \quad (27)$$

This result, as mentioned above is dependent on the choice of zero-order basis functions made.

For completeness we include the $\mathbf{K} \cdot \mathbf{A}$ term

$$\mathcal{K}_{K2}' = \frac{1}{2}(\beta_0/\mu_x)K_y[(\mu_x/\mu_z)^{\frac{1}{2}}zH_x - xH_z] \quad (28)$$

for light propagation in the y direction. In the case $\mathbf{H} \| \mathbf{C}$ the selection rules for this operator are

$$l_i - l_j = \pm 1; \quad m_i - m_j = \pm 1,$$

such that in this configuration one expects the $2S$ and $2P_{\pm 1}$ states to be mixed. Considering the band extrema to lie at $\mathbf{K} = 0$,

$$K_y = n2\pi/\lambda,$$

where n is the index of refraction (in CdSe $n \approx 2.2$ in the optical region) and λ is the wavelength of the incident light. For the $n_1 = 2$ state, the matrix elements connecting the $2P_{\pm 1}$ states with the $2S$ states are about $\frac{1}{4}$ the magnitude of those causing the linear Zeeman splitting of the $2P_{\pm 1}$ states. One would thus suspect that, due to this mixing, the $2S$ state would become observable at high fields in $\mathbf{E} \| \mathbf{C}$. However, we have seen only the $2S_L$ longitudinal exciton state in this polarization identified by the fact that its intensity vanishes when the light is incident exactly perpendicular to the crystal C axis.[16] Thus an upper bound is placed experimentally on the magnitude of this matrix element warranting our neglect of it in the energy calculations.

The energies of the exciton states of principle quantum number $n_1 = 1$, 2 of the first series, in the presence of an external magnetic field both along z ($\mathbf{H} \| \mathbf{C}$) and along x ($\mathbf{H} \perp \mathbf{C}$) have been obtained to first order. The hydrogenic states $\Psi_j(x,y,z)$ and the corresponding exciton energies for $\mathbf{H} \| \mathbf{C}$ are given for observable states in Table I.

One should recall[4] that the wave function associated with the exciton is

$$\Psi_{\text{ex}} = \sum_{K_e, K_h} \chi_{K_e, K_h}^{(K, n)} \psi_{K_e}(r_e)\psi_{K_h}(r_h),$$

where ψ_{K_e} and ψ_{K_h} are Block functions associated with the conduction and valence bands and $\chi_{K_e, K_h}^{(K, n)}$ is the Fourier transform of

$$\chi = e^{i\mathbf{K} \cdot \mathbf{R}}\chi(r).$$

Now it is $\chi(r)$ which satisfies the equation

$$\mathcal{K}\chi(r) = E\chi(r)$$

[16] J. J. Hopfield and D. G. Thomas, J. Phys. Chem. Solids 12, 276 (1960).

TABLE I. Eigenfunctions and energies for $H\|C$ first series $n_1=1, 2,$.

State	C_{6v}	Observed	Function	Energy[a]
$1S$	Γ_5	$E\perp C$	$R_{1s}Y_0^0/\alpha_h\beta_e$	$E_1^0[1+\frac{1}{3}\alpha+(3/20)\alpha^2]+\sigma H_z^2+\frac{1}{2}(g_{hz}-g_{ez})\beta_0 H_z$
			$R_{1s}Y_0^0/\beta_h\alpha_e$	$E_1^0[1+\frac{1}{3}\alpha+(3/20)\alpha^2]+\sigma H_z^2-\frac{1}{2}(g_{hz}-g_{ez})\beta_0 H_z$
$2S$	Γ_5	$E\perp C$	$R_{2s}Y_0^0/\alpha_h\beta_e$	$E_2^0[1+\frac{1}{3}\alpha+(3/20)\alpha^2]+14\sigma H_z^2+\frac{1}{2}(g_{hz}-g_{ez})\beta_0 H_z$
			$R_{2s}Y_0^0/\beta_h\alpha_e$	$E_2^0[1+\frac{1}{3}\alpha+(3/20)\alpha^2]+14\sigma H_z^2-\frac{1}{2}(g_{hz}-g_{ez})\beta_0 H_z$
$2P_0$	Γ_5	$E\perp C$	$R_{2p}Y_1^0/\alpha_h\beta_e$	$E_2^0[1+\frac{3}{5}\alpha+(9/28)\alpha^2]+6\sigma H_z^2+\frac{1}{2}(g_{hz}-g_{ez})\beta_0 H_z$
			$R_{2p}Y_1^0/\beta_h\alpha_e$	$E_2^0[1+\frac{3}{5}\alpha+(9/28)\alpha^2]+6\sigma H_z^2-\frac{1}{2}(g_{hz}-g_{ez})\beta_0 H_z$
$2P_{\pm 1}$	Γ_5	$E\perp C$	$R_{2p}Y_1^{-1}/\alpha_h\alpha_e$	$E_2^0[1+\frac{1}{5}\alpha+(9/140)\alpha^2]+12\sigma H_z^2-[1/\Delta_x-\frac{1}{2}(g_{hz}+g_{ez})]\beta_0 H_z$
			$R_{2p}Y_1^1/\beta_h\beta_e$	$E_2^0[1+\frac{1}{5}\alpha+(9/140)\alpha^2]+12\sigma H_z^2+[1/\Delta_x-\frac{1}{2}(g_{hz}+g_{ez})]\beta_0 H_z$
$2P_{\pm 1}$	$\Gamma_1-\Gamma_2$	$E\|C$	$R_{2p}Y_1^{-1}/\alpha_h\beta_e$	$E_2^0[1+\frac{1}{5}\alpha+(9/140)\alpha^2]+12\sigma H_z^2-[1/\Delta_x-\frac{1}{2}(g_{hz}-g_{ez})]\beta_0 H_z$
			$R_{2p}Y_1^1/\beta_h\alpha_e$	$E_2^0[1+\frac{1}{5}\alpha+(9/140)\alpha^2]+12\sigma H_z^2+[1/\Delta_x-\frac{1}{2}(g_{hz}-g_{ez})]\beta_0 H_z$

[a] Where $\sigma = \frac{1}{4}(e^2/mc^2)a_0^2(e^2/\mu x^3)\eta$.

in the absence of a magnetic field. We have chosen the functions $\Phi(r)$ as zero-order approximations to the $\chi(r)$ and included the electron and hole spin indices to take into account the band splitting in the presence of a magnetic field. To obtain optical selection rules one must, of course, consider the transformation properties of the functions Ψ_{ex}. In Table I we give the irreducible representations, Γ, of the group C_{6v} (transition between states at $K=0$) corresponding to the functions Ψ_{ex}, for those states observable by dipole radiation. The energies of observable exciton states for $H\perp C$ are given in Table II. Note that the S states in this table will be observed only in the polarization $E\perp C$. With $H\perp C$ the spin contribution of the hole is approximately zero ($g_{hx}\approx 0$), since the valence band splitting is large compared to the spin magnetic energies effectively quenching the hole spin along the crystal C axis. Only the exciton states of principle quantum number $n_1=1$, 2 are treated since an essentially different approach must be used for higher n states. This is due to the fact that the large exciton radius for these states

results in magnetic field perturbations, through the diamagnetic, $\mathfrak{K}_3$, term which strongly mix states of different principle quantum number. Already in the $n_1=2$ states this mixing is observed. The mixing through this term between the $n_1=2$ and $n_1=3$ states has been calculated and included in the theoretical curves but not in the tables. A deviation between theory and experiment still exists at high fields indicating that the mixing between the $n_1=2$ and still higher states is becoming considerable.

EXPERIMENTAL PROCEDURE

The experiments were performed on CdSe single crystal platelets of 0.5 to 5 μ thickness with the crystal C axis (i.e., z) in the plane of the platelet. The crystals, mounted strain free, were immersed in liquid helium at 1.8°K or lower for all experiments. A concave grating spectrograph in a stigmatic Wadsworth mounting was used in the second order. The dispersion is about 2.1

TABLE II. Energies for $H\perp C$ first series $n_1=1, 2,$.

State	Energy[a]
$1S^+$	$E_1^0[1+\frac{1}{3}\alpha+(3/20)\alpha^2]+(\mu_x/\mu_z)\sigma H_x^2+\frac{1}{2}g_{ex}\beta_0 H_x$
$1S^-$	$E_1^0[1+\frac{1}{3}\alpha+(3/20)\alpha^2]+(\mu_x/\mu_z)\sigma H_x^2-\frac{1}{2}g_{ex}\beta_0 H_x$
$2S^+$	$E_2^0[1+\frac{1}{3}\alpha+(3/20)\alpha^2]+14(\mu_x/\mu_z)\sigma H_x^2+\frac{1}{2}g_{ex}\beta_0 H_x$
$2S^-$	$E_2^0[1+\frac{1}{3}\alpha+(3/20)\alpha^2]+14(\mu_x/\mu_z)\sigma H_x^2-\frac{1}{2}g_{ex}\beta_0 H_x$
$2P_x^+$	$E_2^0[1+\frac{1}{5}\alpha+(9/140)\alpha^2]+6(\mu_x/\mu_z)\sigma H_x^2+\frac{1}{2}g_{ex}\beta_0 H_x$
$2P_x^-$	$E_2^0[1+\frac{1}{5}\alpha+(9/140)\alpha^2]+6(\mu_x/\mu_z)\sigma H_x^2-\frac{1}{2}g_{ex}\beta_0 H_x$
$2P_y^+$	$E_2^0[1+\frac{2}{5}\alpha+(27/140)\alpha^2]+12(\mu_x/\mu_z)\sigma H_x^2+\frac{1}{2}g_{ex}\beta_0 H_x+\pi$
$2P_y^-$	$E_2^0[1+\frac{2}{5}\alpha+(27/140)\alpha^2]+12(\mu_x/\mu_z)\sigma H_x^2-\frac{1}{2}g_{ex}\beta_0 H_x+\pi$
$2P_z^+$	$E_2^0[1+\frac{2}{5}\alpha+(27/140)\alpha^2]+12(\mu_x/\mu_z)\sigma H_x^2+\frac{1}{2}g_{ex}\beta_0 H_x-\pi$
$2P_z^-$	$E_2^0[1+\frac{2}{5}\alpha+(27/140)\alpha^2]+12(\mu_x/\mu_z)\sigma H_x^2-\frac{1}{2}g_{ex}\beta_0 H_x-\pi$

[a] Where

$$\pi = \left\{\left[E_2^0\left(\frac{1}{5}\alpha+\frac{9}{70}\alpha^2\right)\right]^2+\frac{a^2\beta_0^2}{\Delta_x^2}H_x^2\right\}^{\frac{1}{2}}$$

$$\sigma =\frac{1}{4}\frac{e^2}{mc^2}a_0^2\frac{e^2}{\mu x^3}\eta \qquad a =\frac{1}{2}\left(\frac{\mu_z}{\mu_x}\right)^{\frac{1}{2}}\left(\frac{\Delta_x}{\Delta_z}+\frac{\mu_x}{\mu_z}\right).$$
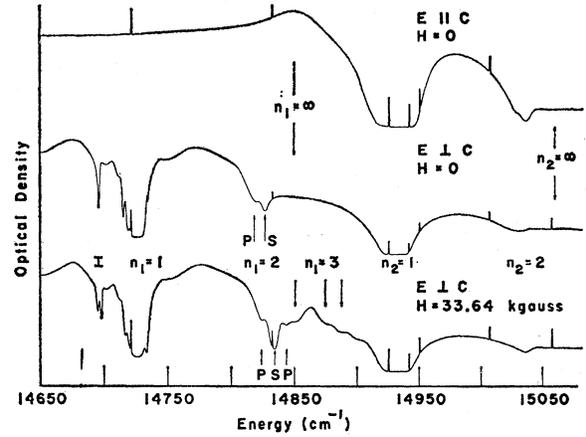
FIG. 2. The spectra observed for a 0.5-μ crystal. The unlabeled lines at energies less than the $n_1=1$ are due to impurity excitons. These and other lines observable in other crystals are variable from crystal to crystal. The calibration emission lines are iron lines third-order, which overlap the second-order absorption spectra.
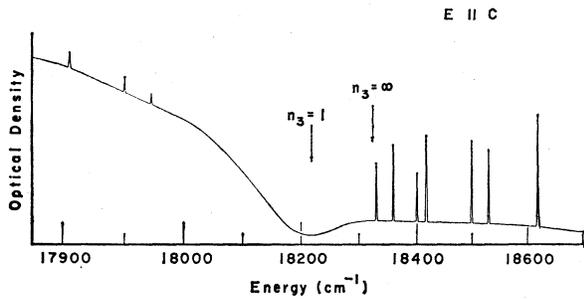
FIG. 3. This spectra indicates the $n_3 = 1$ line of the third series as observed with the same crystal as in Fig. 2. This spectrum however was taken in the first order. We have observed this line only with the very best strain free extremely thin crystals.

A/mm with a measured resolving power using 103a-F Kodak spectrographic plates of greater than 70 000. The magnet was calibrated to 0.1% with current stability of the order of one part in 10^5. Emission lines from various sources were imposed on each plate for calibration purposes. The spectrum was obtained from the plates by a recording densitometer.

EXPERIMENTAL RESULTS AND INTERPRETATION

Typical absorption spectra observed for a single crystal about 0.5 μ thick are shown in Figs. 2 and 3. A reflection spectra for a thicker crystal is shown in Fig. 4. This data gives evidence for three exciton series which we associate with a single Γ_7 conduction band and the three valence bands. Within a given exciton series, one not only expects nearly hydrogen-like energy spacing but also that the intensities will fall approximately as n^{-3}.[17,18] With reference to the group theoretical selection rules of Fig. 1, the band symmetries are obtained from the observed optical selection rules of the exciton $1S$ states. The excited exciton states of
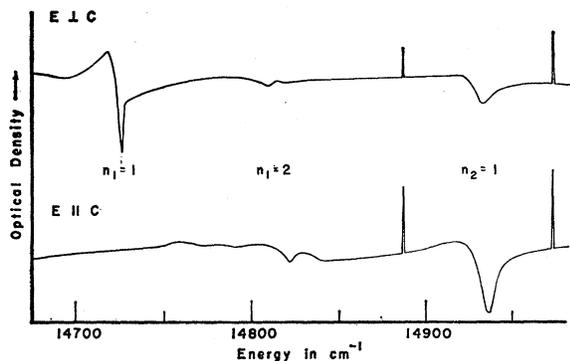
FIG. 4. The reflection spectra in both polarizations from a thicker crystal than that of Figs. 2 and 3 is given. This, as well as the absorption data, indicates that the first series results from a $\Gamma_7 - \Gamma_9$ transition and that the second series results from a $\Gamma_7 - \Gamma_7$ transition.

[17] G. Dresselhaus, Phys. Rev. 106, 76 (1957).
[18] R. J. Elliott, Phys. Rev. 108, 1384 (1957).

the first and the second series are sufficiently narrow to allow one to obtain information from observed magnetic field effects. We shall discuss now the first series (see Fig. 5). The discussion of the second series is facilitated by the use of the band parameters obtained from the interpretation of the first series.

The experimental energies of the excited states of the first series, Γ_9, and the identification thereof, as made by the selection rules and magnetic splittings, are shown in Figs. 6 and 7 for $\mathbf{E}\|\mathbf{C}$ and the two magnetic field orientations and in Fig. 8 for $\mathbf{H}\|\mathbf{C}$ and $\mathbf{E}\perp\mathbf{C}$. As is apparent from the figures, the $n_1 = 3$ and higher states have energies at high fields larger than the zero field series limit. Such lines in the past have been usually identified with transitions between "Landau" levels in the conduction and valence bands. With the polarization $\mathbf{E}\|\mathbf{C}$, (Fig. 6) at zero magnetic field one
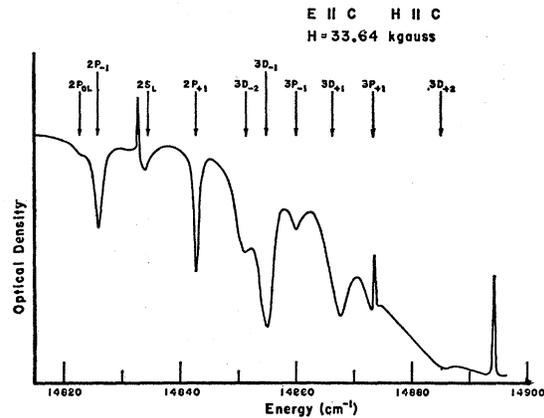
FIG. 5. The excited exciton states of the first series are shown $\mathbf{E}\|\mathbf{C}$ and $\mathbf{H}\|\mathbf{C}$. The spectra was taken with the crystal oriented such that the light vector was not perpendicular to the crystal C axis. The misalignment was about $5°$. The lines labeled $2P_{0L}$ and $2S_L$ are not observed when the crystal is aligned properly. Recall that the zero field series limit is 14 850 cm^{-1}. The crystal from which this spectrum was obtained was thicker than that of Figs. 2 and 3 but not as thick as that of Fig. 4.

expects to observe only Γ_1 exciton states. As indicated in Fig. 1, only one of the $n_1 = 2$ states will be observed. Application of the magnetic field, $\mathbf{H}\|\mathbf{C}$, mixes the Γ_1 and Γ_2 states (which are accidentally degenerate) giving the characteristic linear splitting. From the large diamagnetic shift of these states one may determine the reduced exciton mass μ_x (refer to Table I).[19] With $\mathbf{H}\perp\mathbf{C}$ and $\mathbf{E}\|\mathbf{C}$ (Fig. 7) the Γ_1 and Γ_2 $2P_{\pm1}$ states are mixed with the Γ_5 P_0 state, allowing the latter state to be observed. The zero-field energy for the $2P_0$ state is determined by extrapolation. The $2P_0$ and $2P_{\pm1}$ zero field splitting determines the anisotropy α, and hence measures the ratio μ_x/μ_z. This ratio is also determined independently by comparing the diamagnetic shift of

the $2P$ states with $\mathbf{H}\|\mathbf{C}$ to that with $\mathbf{H}\perp\mathbf{C}$, as indicated in Table II. These two determinations of this ratio are in excellent agreement as shown in the Appendix. At this point one can calculate the series limit and the energies of the $n_1=1$ and $n_1=3$ states. The theoretical and experimental values are given in the Appendix.

The determination of the band mass parameters and g values rests largely upon the linear Zeeman effects. In a magnetic field $\mathbf{H}\|\mathbf{C}$ the only difference between the splittings within the ellipsoidal model of the $2P_{\pm1}$ states with symmetries $\Gamma_1-\Gamma_2$ and those with the
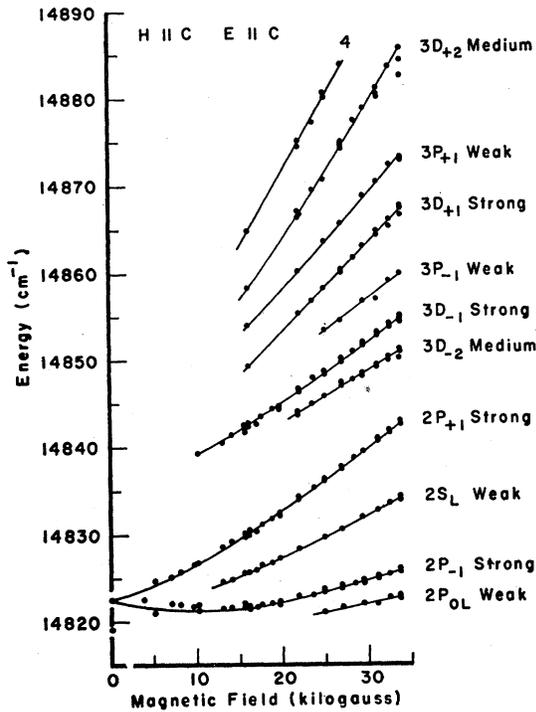
FIG. 6. The energies of the excited exciton states of the first series are plotted against magnetic field with the field and polarization parallel to the crystal C axis. In all cases the propagation direction of the light was nearly normal to the plane of the platelet and normal to the field. This figure includes data from three crystal samples. The lines labeled $2S_L$ and $2P_{0L}$ have the properties as described by Hopfield and Thomas for longitudinal excitons. That is their intensity is dependent upon the orientation of the light propagation vector relative to the C axis. When these vectors are exactly perpendicular the line is unobservable.

symmetry Γ_5 is in the sign of the contribution of the electron spin magnetic moment. This difference in splitting is a measure of the electron g value parallel to the crystal C axis. If one could observe the splitting of the $2S$ state all g values could be determined. From the linewidth, at high field, we determine the upper bound $|g_{ez}-g_{hz}|<1.0$ thus allowing an estimate of Δ_x. By comparing the value of Δ_x with that of μ_x one obtains the transverse hole and electron effective masses. We have assumed that the effective mass of the hole is greater than that of the electron as is reasonable.
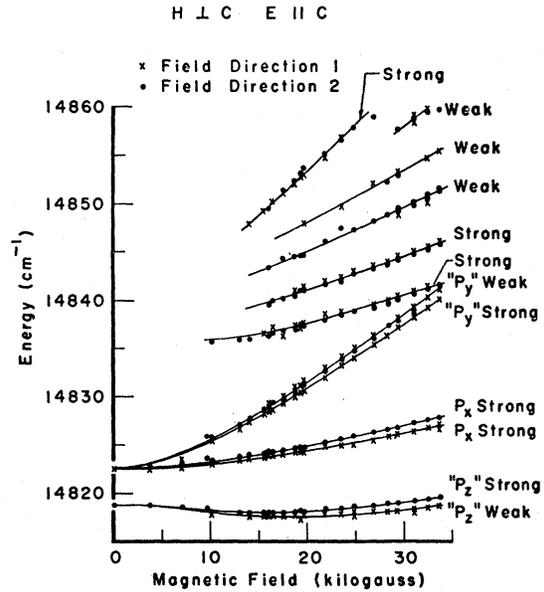
FIG. 7. The energies of the excited exciton states of the first series are plotted against magnetic field with the field perpendicular and the polarization parallel to the crystal C axis. The propagation direction of the light was normal to the plane of the crystal platelet and normal to the field. This figure includes data obtained from three crystal samples.

With the magnetic field perpendicular to the C axis a determination of the longitudinal mass parameters can be obtained. A plot of π^2 vs H^2 theoretically yields a straight line of slope $(a\beta_0/\Delta_x)^2$ (see Table II). π can be obtained by comparing the energies of observed
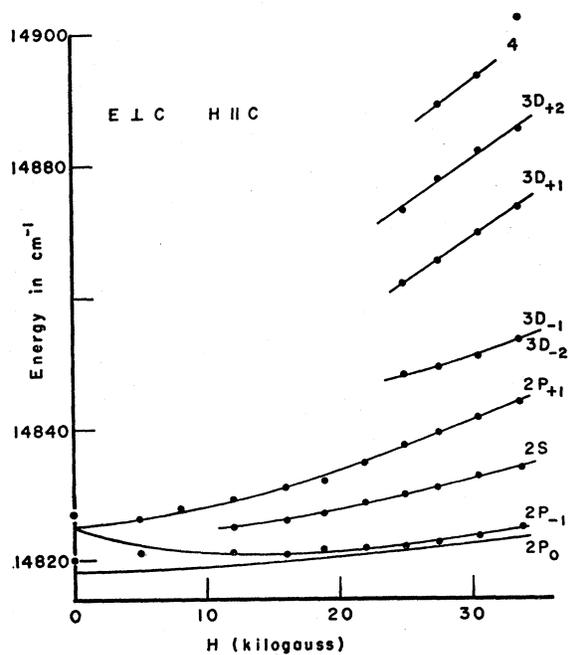
FIG. 8. The energies of the excited exciton states of the first series are plotted against magnetic field with $\mathbf{E}\perp\mathbf{C}$ and $\mathbf{H}\|\mathbf{C}$. This figure includes data from two crystal samples.
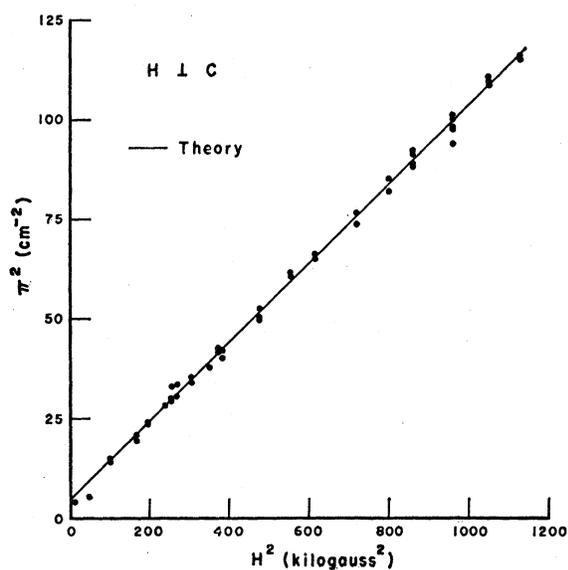
FIG. 9. The quantity π^2 (see Table II) obtained experimentally from

$$\pi^2 = \tfrac{1}{4}[E(2P_y{}^{\pm}) - E(2P_z{}^{\pm})]^2$$

is plotted against H^2. The straight line drawn through that data points has the theoretical slope $(a\beta_0/\Delta_x)^2$ and intercept

$$\{E_2{}^0[\tfrac{1}{3}\alpha + (9/70)\alpha^2]\}^2.$$

The fact that the data points do fall rather close to a straight line shows a striking agreement between theory and experiment.

states. In Fig. 9 we have plotted the experimental values of π^2 against H^2 and used the slope of the resultant straight line to determine a, and thus the longitudinal band parameters. The small energy difference between the two cases of H along x and H along $-x$ may be ascribed to the transverse electron spin energy. As previously mentioned the transverse hole spin g value is very small.

The parameters obtained have been used to calculate the energies, with $H\|C$ and $H\perp C$, of all observable $n_1 = 1$, 2 states, both $E\|C$ and $E\perp C$. The results of these calculations are plotted in Figs. 10 and 11 along with the experimental data. The theoretical curve for the $2S$ state lies uniformly about 1 cm^{-1} below the experimental points. It should be noted that this curve has been shifted upwards by 1 cm^{-1} in Fig. 10. As will be discussed later this and other effects may be caused by the presence of toroidal energy surfaces. Due to the linewidths, the P_{-1} and P_0 Γ_5 states in a magnetic field cannot be resolved, however the observed resultant line is in good agreement with prediction. From the $E\perp C$ data only the electron spin g value was determined.

Agreement with the ellipsoidal model appears to be poor for the Γ_5 states at zero field. We observe only two lines, $E\perp C$, one located at the expected position of the $2P_0$ state and the other approximately 4 cm^{-1} higher than the extrapolated energy of either the Γ_5 $2S$

or $2P_{\pm 1}$ states. Casella[20] has made preliminary calculations including the possibility of conduction band toroidal energy surfaces as a perturbation to the ellipsoidal model. The preliminary results indicate that at zero field the splittings between the $2S$ and $2P_{\pm 1}$ Γ_5 states should be in excess of that predicted by the ellipsoidal model, and that these states are mixed with each other. It is felt that no conclusions may be drawn at this time.

The higher states of the first series as observed in a magnetic field must be analyzed by the method of Elliott and Loudon.[21] The identification is easily made by comparison with their theory at high fields, and by using the optical selection rules and the predictions of the ellipsoidal model, with the band parameters obtained from the analysis of the $n_1 = 2$ states, at low fields.

Some comments need to be made concerning intensities. In general with magnetic field the intensities of all exciton lines increase. The $n_1 = 3$ and higher excited states usually cannot be observed at zero field. This increase in intensity is to be expected,[21,22] from the large diamagnetic effect upon the exciton orbits. The most striking intensity effects, as indicated in Fig. 12, occur with the magnetic field perpendicular to the C axis. Due to the finite wavelength of the light and the
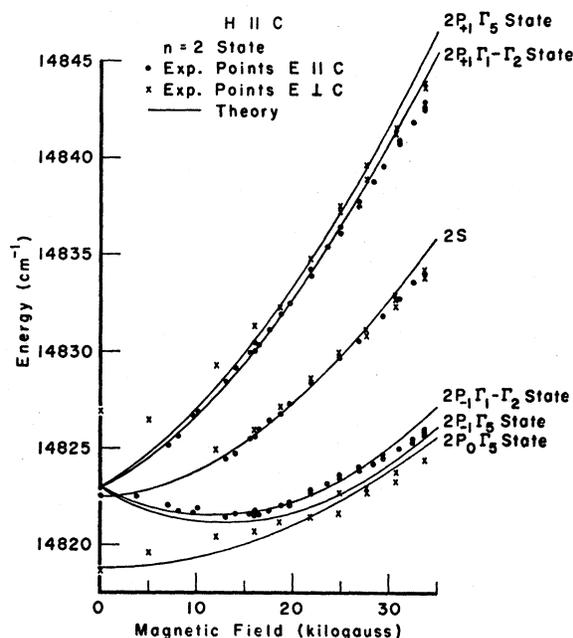
FIG. 10. The $n_1 = 2$ states with the magnetic field along the C axis are shown in both polarizations as compared with the theory. Only the data of the P states is used to determine the parameters ncecessary for the theoretical predictions.

[20] R. C. Casella (private communication).
[21] R. J. Elliott and R. Loudon, J. Phys. Chem. Solids 15, 196 (1960).
[22] J. J. Hopfield, Reported at the Conference on Semiconducting Compounds, Schenectady, New York, 1961, J. Appl. Phys. Suppl. 32, 2277 (1961).
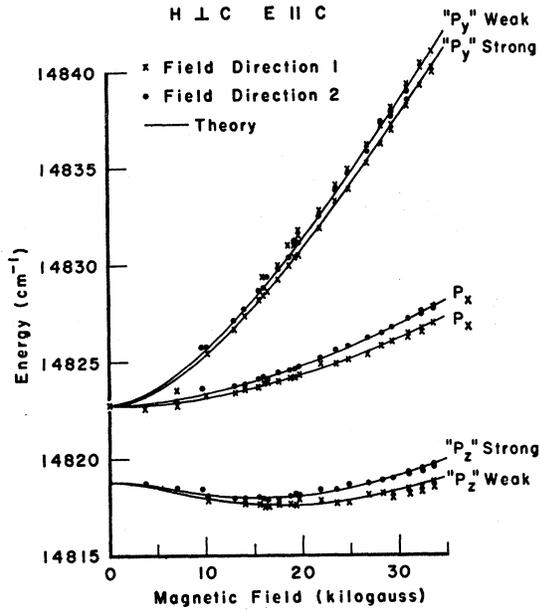
FIG. 11. The $n_1=2$ states are shown in the $E\|C$, $H\perp C$ configuration as compared with the theory. Photon momentum effects are observed in this configuration similar to those reported for CdS by Hopfield and Thomas.

lack of inversion symmetry, one set of the $n_1=2P$ states has a large intensity with the field in one direction, the other set with the field in the opposite direction. The energy difference between respective components is due to the transverse electron magnetic moment contribution. The details of this intensity pattern are the same as for CdS given by Hopfield[23,24] and thus will not be reiterated here.

The interpretation of the data is more difficult for the excited states of the second series than for the first series. The lines are broader by approximately a factor of 3 and the intensities are considerably less. With these experimental limitations in mind we have made the following interpretation. As indicated in Fig. 1, the $2S$, $2P_0$ and $2P_{\pm 1}$ states may be observable in both polarizations. Assuming the applicability of an ellipsoidal model for these states, the data of Fig. 13 indicates that the $2P_{\pm 1}$ state lies higher than the $2P_0$ state.

Due to the large anisotropy apparent in this series the perturbation calculation is not valid, but rather a variation approach is necessary. However, the experimental zero field splitting indicates an effective mass ratio, μ_z/μ_x, greater than in the first series. An alternative interpretation is that the large zero-field splitting observed is due to the fact that in this case the energies of both the conduction and valence bands may contain terms linear in wave vector at $K=0$.

[23] J. J. Hopfield and D. G. Thomas, Phys. Rev. Letters 4, 357 (1960).
[24] J. J. Hopfield and D. G. Thomas, Phys. Rev. 122, 35 (1961).

As indicated in Fig. 6, states are observed in $E\|C$ radiation which do not obey the dipole selection rules for $K=0$. These lines, labeled P_{0L} and S_L, are observed only when the light is not incident exactly perpendicular to the C axis. Their intensity increases with increasing deviation from perpendicularity. This is just the description of Hopfield and Thomas[16] for the longitudinal exciton. The $1S_L$ exciton, associated with the ground state, has been observed at 14 730 cm^{-1}. Other absorption lines have been observed always at lower energies than the ground state, that is, at higher binding energies. We have found that these lines are variable in intensity from crystal to crystal. Further, they have associated nearly always the same linear Zeeman effect with $|g_{11}|=1.65$ $|g_{\perp}|=0.5$. Thus we attribute these lines to excitons associated with impurities and defects in the crystal.

As pointed out by Roth[11,12] one may use the effective mass formalism to calculate from known band symmetries, energies and effective masses, the electron g value associated with the conduction band. For CdSe we have found the electron effective mass to be nearly isotropic and the crystal field splitting in the valence band to be very small compared both with the spin-orbit splitting and with the band gap. With these considerations it appears that Eq. (A5) of Roth et al.,[11] may be applied to the case at hand if we assume that only the bands discussed contribute to the relevant matrix elements. These assumptions imply a nearly isotropic electron g value. In the present notation this equation reads

$$g_e - 2 = -\left(\frac{m}{m_e^*} - 1\right)\frac{2E_{so}}{3E_g + 2E_{so}}, \qquad (29)$$

where E_g is the band gap and E_{so} is the spin-orbit
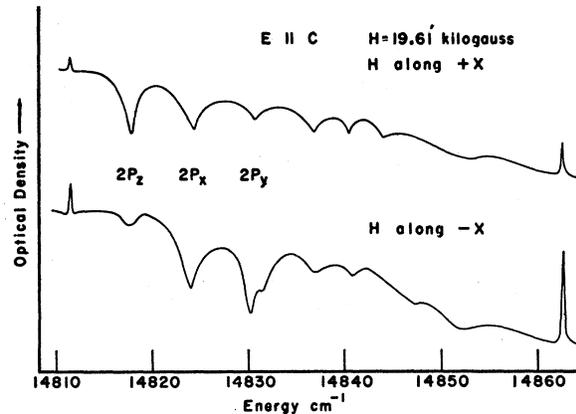
FIG. 12. Densitometer traces are shown of the excited states of the first series $E\|C$ and $H\perp C$ for H along $+x$ and for H along $-x$. Note the large intensity changes in the $2P_z$ and $2P_y$ states upon reversal of the field. The $2P_y$ state observed with H along $+x$ corresponds in energy to the higher energy shoulder on the $2P_y$ absorption line observed with H along $-x$.
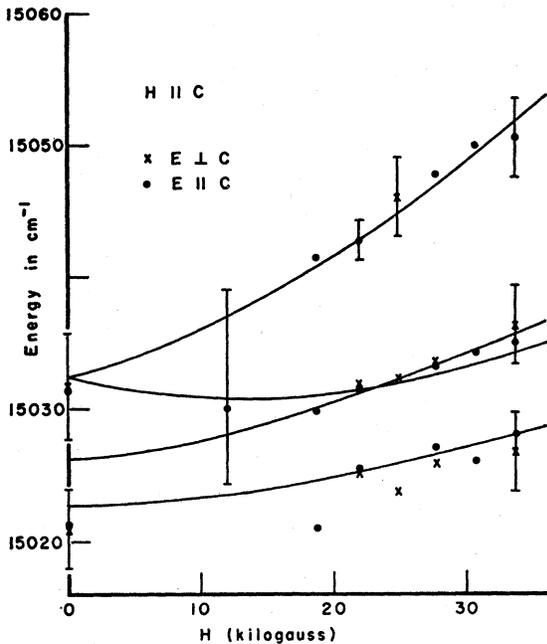
FIG. 13. The experimental points and curves for the $n_2=2$ states of the second series are plotted against magnetic field with $H\|C$ and both $E\|C$ and $E\perp C$. The error bars in the figure indicate the experimental linewidths for the various lines at different magnetic field strengths. It was noted that as the magnetic field strength increased the linewidths decreased and the line strengths increased. This was true in general except for S states.

splitting of the valence band. Using $m_e^*=0.13$ m, $E_{so}=3500$ cm^{-1} and $E_g=15\,000$ cm^{-1}, Eq. (29) gives $g_e\simeq+1.1$. The value deduced from the Γ_5, $\Gamma_1-\Gamma_2$ $2P_{\pm 1}$ state splitting using the ellipsoidal model and the assumption that $m_{ex}^*<m_{hx}^*$ is $g_e=-0.6\pm0.1$. We believe that the assumption is valid and that the application of Eq. (29) to CdSe should give roughly the correct result. This may suggest that either the identification of the Γ_5 $2P_{\pm 1}$ state is in error or that conduction band toroidal energy surfaces have lifted the accidental degeneracy of the Γ_5 and $\Gamma_1-\Gamma_2$ $2P_{\pm 1}$ states present in the ellipsoidal model at zero field.

CONCLUSION

The ellipsoidal model has allowed us to interpret the observed exciton spectra of CdSe and to obtain the effective mass parameters of the conduction and valence bands. Good quantitative agreement is obtained with the few exceptions mentioned above. These possibly may be attributed to toroidal energy surfaces. The significant difference between this spectra and that of CdS,[24,25] is that in CdSe the crystal field splitting is greater than the exciton binding energy while in CdS

[25] R. G. Wheeler and J. O. Dimmock, Bull. Am. Phys. Soc. Ser. II, **5**, 178 (1960).

it is not. Thus one would expect much less valence band mixing due to the exciton states in CdSe than in CdS. This is evidenced by the fact that transitions are observed in CdS forbidden by the group theoretical optical selection rules considering isolated bands, while in CdSe only allowed transitions are observed.

APPENDIX

Series I

From the $H\|C$ diamagnetic shift we determine the reduced effective mass of the exciton in the x direction,

$$\mu_x=0.100\pm0.005.$$

The relative zero field positions of the $n_1=2$ states gives us a measure of the anisotropy parameter.

$$\alpha=0.32\pm0.02.$$

Now since $\alpha=(1-\mu_x\epsilon_x/\mu_z\epsilon_z)$ and we know the values of ϵ_x and ϵ_z ($\epsilon_x=9.7$, $\epsilon_z=10.65$) this gives

$$\mu_x/\mu_z=0.75\pm0.04.$$

The comparison of the $H\perp C$ diamagnetic shift with the $H\|C$ diamagnetic shift gives

$$\mu_x/\mu_z=0.77\pm0.04$$

in good agreement with the anisotropy determination. From either of these we have $\mu_z=0.13\pm0.01$. The effective Rydberg for this series is 106 ± 5 cm^{-1}, and the series limit, hence the band gap, is $E_g=14\,850$ ±2.0 cm^{-1}. The effective Bohr radius $a_0'=54$ A. Using these numbers the $n_1=1$ and $n_1=3$ states may be compared with that experimentally observed.

State	Experimental	Calculated
$1S$	$14\,727\ \pm1$ cm^{-1}	$14\,736\ \pm6$ cm^{-1}
$2P_0$	$14\,818.6\pm0.3$ cm^{-1}	
$2P_{\pm 1}$	$14\,822.5\pm0.2$ cm^{-1}	
$3P_{\pm 1}$	$14\,839\ \pm1$ cm^{-1}	$14\,838.0\pm1.5$ cm^{-1}

The band mass parameters and electron g values are

$$m_{ex}^*=0.13\pm0.01\ m \qquad m_{hx}^*=0.45\pm0.09\ m$$
$$m_{ez}^*=0.13\pm0.03\ m \qquad m_{hz}^*\geq m$$
$$|g_{ex}|=0.51\pm0.05 \qquad |g_{ez}|=0.6\pm0.1$$

There is some evidence that the electron g values are negative. The Zeeman splitting between the $2P_{+1}$, $\Gamma_1-\Gamma_2$ and Γ_5 states indicates a negative g_{ez}.

Series II

The experimentally observed states and their energies are

State	Energy
$1S$	$14\,931\pm3$ cm^{-1}
$2S-2P_{\pm1}$	$15\,032\pm2$ cm^{-1}
$2\,P_0$	$15\,022\pm3$ cm^{-1}

The series limit may be estimated to be $15\,050\pm15$ cm^{-1} with an effective rydberg of $Ry=120\pm10$ cm^{-1}.

Series III

The $1S$ state was observed at $18\,218\pm10$ cm^{-1}, with an estimated series limit at $18\,340\pm20$ cm^{-1}.

The difference in the series limits between the first and second series corresponds to a crystal field splitting of the valence band of 200 ± 15 cm^{-1}. The difference between the limits for the first and third series corresponds to a spin-orbit splitting of the valence band of 3490 ± 20 cm^{-1}.

Interband Electron-Electron Scattering and Transport Phenomena in Semiconductors

Joachim Appel

John Jay Hopkins Laboratory for Pure and Applied Science, General Atomic Division of General Dynamics Corporation, San Diego, California

(Received November 6, 1961)

The effect of interband electron-electron scattering (electron-hole scattering, light hole–heavy hole scattering, etc.) on the electrical transport phenomena is studied with a variational method obtained by a generalization of Kohler's variation principle to a multiband conductor. To this end we make the following assumptions: (1) The electronic structure is given by parabolic conduction and valence bands, separated from each other by $\Delta E \gg k_B T$; the valence band may be twofold degenerate; (2) The average occupation numbers of electronic eigenstates are given by Fermi-Dirac statistics; (3) The dynamical interaction between charge carriers is described by a shielded Coulomb potential.

Assuming nondegenerate semiconductors, we consider acoustical and optical phonon scattering and ion scattering, besides electron-electron scattering. Quantitative results are obtained for the electrical conductivity, the heat conductivity, and the Seebeck coefficient, including the ambipolar effect. The results can easily be applied to cases of physical interest; we discuss here hole-hole scattering and mobility of p germanium, intercarrier scattering and mobility of intrinsic germanium, transient conductivity of charge carriers in germanium produced by short pulses of high-energy electrons, intercarrier scattering and its influence on the heat conductivity, and the Wiedemann-Franz ratio of intrinsic semiconductors.

I. INTRODUCTION

IN a previous paper[1] the effect of electron-electron scattering on the electrical transport phenomena was studied on the basis of the free-electron approximation and under the assumption of a shielded Coulomb potential describing the pair interaction between conduction electrons. The allowed electron eigenstates were restricted to one band only. For such a simple model, because of momentum conservation in a single (non-umklapp) scattering process, the electrical conductivity is not affected in its zero-order approximation. However, in first and higher order, the electrical conductivity changes. The reason for this change lies in the energy dependence of the perturbation f_1, which, as a consequence of the electron-lattice interaction, adds to the unperturbed Fermi-Dirac distribution f_0. The perturbation f_1 is modified because electron-electron scattering randomizes energies. The effect on the electrical conductivity of semiconductors is shown in Fig. 1, assuming electron-ion scattering as the primary scattering source.

The effect of electron-electron scattering becomes more important for the electrical conductivity when the electrons are distributed over two or more partly filled energy bands. Transition metals and intrinsic semiconductors are examples of a multiband structure. In considering the electrical conduction of such substances, it is convenient to distinguish between intraband and interband electron-electron scattering processes. The former have been discussed in A, while the latter may be understood as scattering processes in which each of the two participants belongs to a *different* band (the first to a conduction band, the other to a valence band, etc.). The transition probabilities are the same whether each of the two electrons stays in its original band or whether the two electrons exchange bands. Both direct and exchange transitions will be called interband scattering processes. Physically, the difference between intraband and interband scattering is trivial: In the first case the momentum conservation in a single scattering event implies the velocity conservation $v_1+v_2=v_1'+v_2'$, whereas in the second case usually $v_1+v_2 \neq v_1'+v_2'$. In other words, interband scattering processes affect the electrical conductivity primarily because of a current

---

[1] J. Appel, Phys. Rev. **122**, 1760 (1961), hereafter referred to as A.